Наносистеми, наноматеріали, нанотехнології
Nanosistemi, Nanomateriali, Nanotehnologii
2025, т. 23, № 2, сс. 333–348
https://doi.org/10.15407/nnn.23.02.0333

PACSnumbers: 03.67.Dd, 68.65.Hb, 68.65.La, 73.21.Hb, 73.21.La, 73.63.Kv, 73.63.Nm, 85.35.Be

QCA Nanoarchitecture for Morphological Processes on Binary Images

Nasima Akter[1], Md. Abdullah-Al-Shafi[2], and Md. Nasim Akhtar[1]

[1]*Dhaka University of Engineering & Technology, Gazipur, Bangladesh*
[2]*University of Development Alternative (UODA), Dhanmondi, Dhaka, Bangladesh*

A prospective nanoarchitecture, quantum-dot cellular automata (QCA), provides a novel technique for plotting digital architectures at a minimal scale with substantial advances. It is a promising nanoarchetype with outstanding achievement to challenge the deficiencies of complementary metal–oxide–semiconductor (CMOS) based architecture just as switching speed, design, and fabrication sizes. QCA relies on the manipulation of quantum dots (nanoscale semiconductor particles) to perform computation and store information. Complex image processing approaches take in a number of cases that identified binary median filter and mathematical morphological (MM) procedures, for instance, erosion and dilation. When it comes to MM on binary images, QCA can be used to implement digital image-processing operations. Morphological operations are fundamental in image processing and computer vision for tasks such as noise reduction, object detection, and image enhancement. QCA can provide a platform for designing and implementing efficient morphological operators for binary images. Erosion and dilation are substantial approaches in frequent real-life image appliance. In this research, optimized nanostructures in QCA are outlined for MM applications that function dilation and erosion. The proposed nanoarchitecture is compared with the best counterpart that reveals a substantial advancement with regard to cell operation, extent, and delay. The proposed configurable design achieved 42.20%, 41.18%, 50.00% and 60.84% improvement, and the non-configurable design achieved 12.42%, 31.24%, 34.36% and 12.45% improvement in terms of employed cell, enclosed extent, clock and cell extent, correspondingly. Further, the energy consumption through the structures is assessed at distinct temperatures' level of 2 K.

Перспективна наноархітектура, — квантово-точкові клітинні автомати (КТА), — пропонує новий метод побудови цифрових архітектур у мінімальному масштабі зі значними досягненнями. Це — перспективний

наноархітип з видатними досягненнями у подоланні недоліків комплементарної архітектури на основі метал-оксид-напівпровідників (КМОП), а також у швидкості перемикання, дизайні та розмірах виготовлення. КТА спирається на маніпулювання квантовими точками (нанорозмірними напівпровідниковими частинками) для виконання обчислень і зберігання інформації. Складні підходи до обробки зображень враховують низку випадків, які ідентифікують бінарний медіянний фільтр і математичні морфологічні (ММ) процедури, наприклад, ерозію та дилятацію. Коли справа доходить до ММ на бінарних зображеннях, КТА може бути використана для реалізації операцій цифрової обробки зображень. Морфологічні операції є фундаментальними в обробці зображень і комп'ютерному зорі для таких завдань, як зменшення шуму, виявлення об'єктів і поліпшення зображення. КТА може забезпечити платформу для проєктування та впровадження ефективних морфологічних операторів для бінарних зображень. Ерозія та дилятація є важливими підходами в частому застосуванні реальних зображень. У цьому дослідженні описано оптимізовані наноструктури в КТА для застосувань ММ, що функціонують як дилятація й ерозія. Запропонована наноархітектура порівнюється з найліпшим аналогом, що демонструє істотний проґрес щодо роботи комірки, обсягу та затримки. Запропонована конфіґурована конструкція досягла поліпшення на 42,20%, 41,18%, 50,00% і 60,84%, а неконфіґурована конструкція досягла поліпшення на 12,42%, 31,24%, 34,36% і 12,45% з точки зору використовуваної комірки, обсягу замкнутого простору, тактової частоти та обсягу комірки відповідно. Крім того, споживання енергії структурами оцінюється на різних температурних рівнях у 2 К.

Key words: quantum-dot cellular automata, morphology, erosion, dilation.

Ключові слова: квантово-точкові клітинні автомати, морфологія, ерозія, дилятація.

(Received 18 December, 2023; in revised form, 27 January, 2024)

1. INTRODUCTION

QCA are imminent nanoarchitecture beyond existing changes to encode binary information [1–3]. In CMOS architecture, the computing supremacy has improved drastically throughout the previous 10 years and has been reliant on transistor decline [4–6], and so, improved configurability of CMOS architecture effects the execution of several aspects such as heat depletion and outflow currents [7–9].

Many studies are accepted by researchers to annihilate the limitations of transistor-based architecture. QCA, as one of the resolutions, is an innovative transistor less quantum model with extreme low power dissipation and decidedly small extent [10–13]. The logic statuses of QCA are presented by a cell that is operated to encode and transmit da-

ta through the two state electron arrangements [14–17].

The QCA cell group can be combined and ordered specifically to manage computation functions [18–20]. Image operations is a particularly investigating area in very large-scale integration (VLSI) archetype by reason of its several restrictions in processing power and as yet, this archetype is extensively operated to design the distinction of image operations. In real life image operations, it is recurrently vital to lessen noise level through specific substances of the image need to be sustained to expand the complete effect. A nonlinear filtering approach such as median is adept to exclude coercion noise although alleviating the image thresholds [3].

A familiar nonlinear image operation process is morphology [4] that is placed on the figure of an individual embedded in an image and profoundly linked with the set theory [5] and Minkowski algebra [6]. In the early, MM process was functioned on binary images later, several deviations and generalizations processes have been defined to be practicable on monochrome or pigmented images [7]. Through the usage of complex coding and scripting, there are provisional consequences where binary images emerge. Digital image operation is continuously emergent research part with huge applications spreading out into our life and such utilization embrace several techniques like object realization and image improvement. Recognizing such complex presentations on everyday computer can be adequate, but not decisive due to restrictions on computational memory and peripheral machines [8]. Operating complex computational functions on hardware through pipelining and parallelism in algorithms, return significant falling in execution phases [9].

Emerging nanoarchetypes have been the consideration of comprehensive investigation whereas traditional VLSI archetypes are getting their substantial ceiling. QCA shows a state-of-the-art information presentation system that proposed a systematic digital logic presence and points to the expansion of different design methods [10]. Numerous logic designs and devices are proposed through QCAs, *e.g.*, QCA wire [11], 3-input and 5-input majority logic, XOR circuit [12], several and flip-flops [13–19], several sequential and combinational logic architectures [20–26], and reversible architectures [27, 28].

Now, a number of operations are identified for scientific MM methods with nonlinear filters. A marginal median filter was designed without QCA structure in [29]. This work, two MM filters are outlined focused on circuit functionality where the designed circuits present parallel processing, intense functioning, and minimal energy depletion. Moreover, the designs are developed in reference to cell intricacy, dimension, and latency as associated with the existing layout [30, 33].

The preeminent purpose of this research is described below:
— designing optimal layouts of single layer QCA configurable and non- configurable MM filters to decrease cell complexities and covered area;
— comparing and assessing the presented schematization with existing schematizations;
— investigating and demonstrating the effectiveness of the proposed layouts with the usage of the QCADesigner and QCAPro simulation engine.

In the following Section, a detailed summary of MM operation is systematized. Section 3 provides the relative study of QCA nanoarchetypes, and Sec. 4 presents the performance of the proposed circuits. Energy depletion and output emission by the designed circuits are provided in Sec. 5 and consequently conclusion in Sec. 6.

2. MORPHOLOGICAL TECHNIQUES IN IMAGE OPERATION

A number of shortcomings may enclose in binary images and, in certain contexts, the binary spaces assembled by plain thresholding are distorted by textures. MM process is a substantial choice of image applications that adjusts the binary images based on contours. This operation is measured to be particular data processing techniques convenient in image practices *e.g.*, noise abolition, boundary removal, texture evaluation and more [5]. MM image operations stick to the aim of abolishing the shortcomings and preserving the formation of binary image. The procedures are certain basically on the correlated classifying of pixel values, instead of the statistical values, thus the process realized more on images, nevertheless this process can also be practical to monochrome images where the light transmission is unidentified and therefore the outright picture element are not received in concern [6]. MM procedures substantiate the image through a small prototype called configuring module and this module is practical to all potential settings of the feedback image and produces the similar dimension's output. Within this operation, the producing image picture element values are formed on same picture elements of feedback image through is neighbours. This process shows a new image where if the assessment is positive, it will perform non-null picture elements at that setting in the feedback image. The basis of the MM process is opening, closing, erosion, dilation specified in logical AND, OR representation and defined by set evaluation [6]. The exclusion or addition of picture elements rests on the configuring module that utilized for operating the image.

Erosion is a particular and essential operator in MM and it is the reasons of image lessening or become narrow in dimension. Erosion

is mostly dwindling with the margins of the forefront that outcomes in spaces of those picture elements shorten in dimension and voids of those dimensions converted higher [7]. Thus, after thinning and loading the voids of images, the margins become occupied, hence, to some extent isolated; the margins erosion is practical so as to create the margins of the images narrower for enhanced output [8]. In this process, two elements work as data. The initial one is the feedback image to be eroded and next is the configuring module. Let M be a complete grid and B is an image in M. The mathematical characterization of erosion of B by the configuring module C is recognized by

$$B \ominus C = \{z \in M | C_z \subseteq B\}. \quad (1)$$

In this equation, C_z is the conversion of C through the direction z.

Dilation is another essential process in MM where it is practical not only to binary image but also practical to monochrome image. This operation reasons the image objects to rise in dimensions. The outcome of this process will steadily rise the margins of forefront pixels; hence, spaces rise in dimensions and voids in that dimensions convert smaller [7, 38]. Unlike erosion, the dilation takes has two elements that works as data. The initial one is the feedback image that needs to be dilated and next one is the configuring module also recognized as kernel. The mathematical characterization of dilation of B by C is recognized by

$$B \oplus C = \bigcup_{c \in C} B_c . \quad (2)$$

This operation can also be achieved as follows:

$$B \oplus C = \left\{ z \in M \mid \left(C^z\right)_z \cap B \neq \emptyset \right\}. \quad (3)$$

In this equation, C^s indicates the proportionate of C.

It can be perceived from Fig. 1 that the dilation and erosion model can be noted the previous formation of the image and precisely in what way the procedures of configuring module alter the initial image. During the dilation procedure if the origin of the configuring module overlays through a dark picture element, then spot dark all picture elements from the image surrounded through the module. Wherever the origin of the module overlays with a white one, then adjusts to the subsequent picture element.

Through the erosion operation if the origin of the configuring module overlays through a dark picture element and as a least one of the dark picture elements in the module drops over a white one, then change the dark element in the binary image from dark to

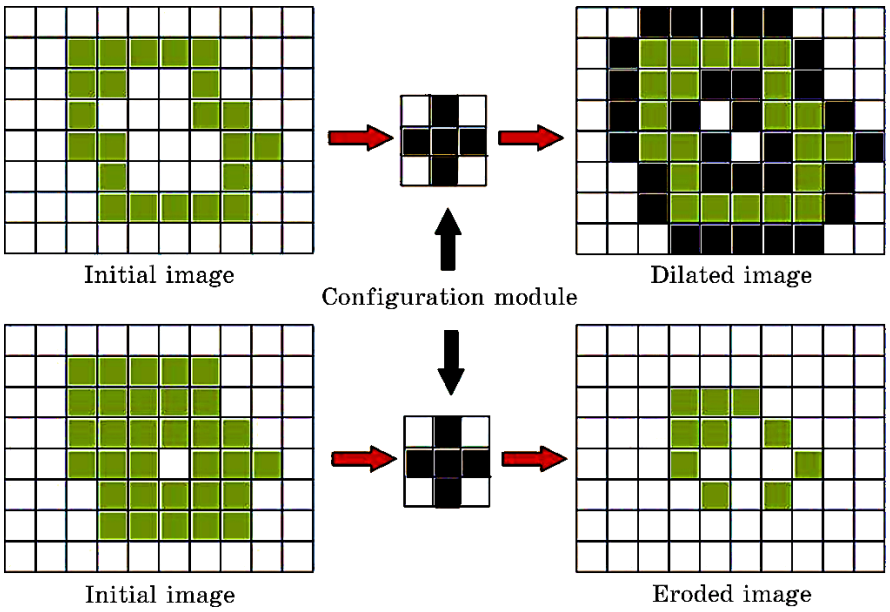

Fig. 1. Dilation and erosion operations by configuring module.

white. Wherever the origin of the module overlays with a white one in the image, then no adjustment is needed, directly adjust to the subsequent picture element.

3. QCA SUMMARY

QCA is a prospective generation nanoarchetype, which signifies logic conditions not as voltage state but relatively as the form of a couple of electrons in a square cell. The square cell is consisting of four dots known as quantum-dots that are employed in the edges of each cell, and two additional movable electrons. The electrons can channel concerning the quantum dots in the square cell, however cannot skip the cell. Then electrons continuously employ the dots at the transversely contrasting edges, because of the coulomb revulsion within the electrons. Therefore, two firm statuses can be shaped in the quantum cell, as indicated in Fig. 2, *a*, logic '0' and logic '1' or polarization −1 and polarization +1, respectively. Information in binary format can be conducted by adjoining cell interfaces along a route of cells that is termed as QCA wire. Another revolved (45°) cells, as exposed in Fig. 2, *b*, for realizing a QCA inverter chain also for crossing resolutions in QCA [9]. In this archetype, almost all designs are executed with inverter gate and majority voters as directed in Fig. 2, *c* and Fig. 2, *d*, correspondingly.

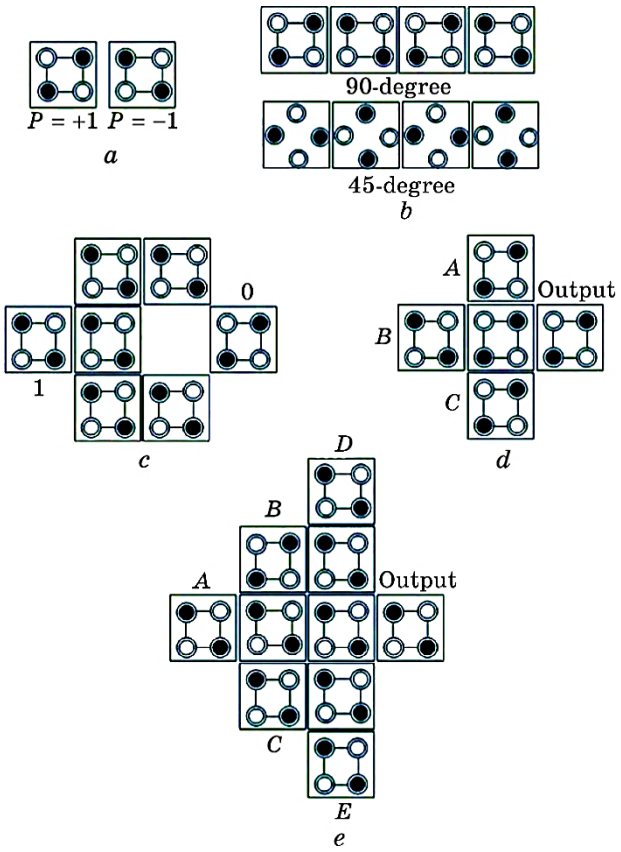

Fig. 2. QCA logical designs: *a*—plain cell; *b*—wires; *c*—potent inverter; *d*—3-input majority gate; *e*—5-input majority gate.

Placing the QCA cells transversely enables the inversion process. A basic majority voter can be executed with five QCA cells. Logical AND or OR designs are arranged by changing particular fixed feedbacks of the gate to logic '0' or logic '1', correspondingly. The settled feedback in the input defines the statues of the others two inputs and it is a condition of the conservative three-input majority voter. A different sort of QCA five-input majority voters is presented in [13–15, 19, 21–23, 37] but the most common is presented in Fig. 2, *e*.

Like the archetypal CMOS layout, the clocking mechanism is a decisive element in all combinational and sequential QCA architectures. The foremost assistance of clocking keeps in the circumstance that information forfeiture and lessening can be re-established. An electric mechanism assists to generate the QCA clocking field [12]. The substantial states specify a benefit to QCA architecture [17];

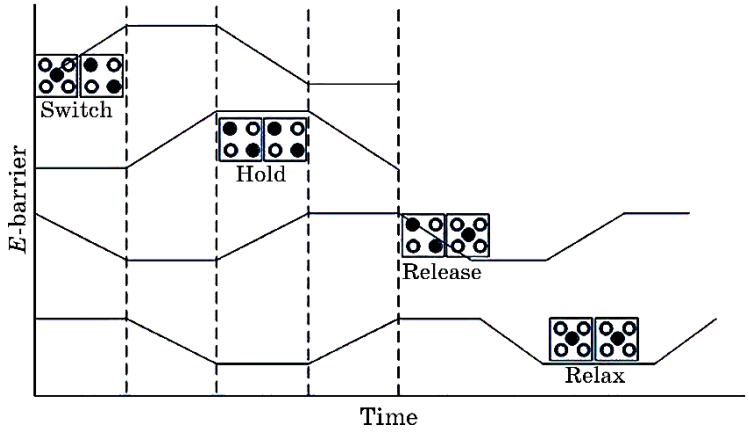

Fig. 3. QCA clocking procedures.

however, it is essential to plot with the consistent clarification of the challenge for which the architecture is intended to resolve. QCA architecture can be in several excited statuses if the feedback of the architecture is moved unexpectedly which directs to a meta-steady situation, and it can initiate interval to attain at its steady ground situation [31]. Accordingly, to evade such complications, adiabatic switching gains the attention. As per the research in Ref. [12], a clock requisite four levels specifically switch, hold, release, and relax as presented in Fig. 3 for an adiabatic sequence. In the initial level, the inter-dot impediments are composed that polarizes the cell. After that in the hold level, the impediments are so elevated that the emission of the cells cannot be altered from an outside origin; therefore, it holds its emission status [31]. The impediments are dropped and the polarization are declines in the release level and in time, the cells turn into un-polarized in the relax level. In every rotation, the neutralized cells are revitalized [17]. The energy depletion is minimal since only two additional electrons are affecting [31, 37].

4. OUTLINED QCA CIRCUIT ARCHITECTURES

It is quite necessary in nanoscale design to propose a structure that can perform with advanced reliability [33]. It has been investigated that easy QCA outlines perform in computer simulation though, break down once it is set to perform as a part of a complex architectures. In other illustrations, the circuit architects that take about their projects to run it in computer simulation, they simply regulate simulation constraints. Hence, a number of circuits are not

practical. This part the designed architectures are provided with applicable outcome. For erosion process, configuring module need to be kept in the feedback image and for dilation process, it needs to be temperately narrowed. At this time, all five-pixel valuation of the image, which drops under the distinct picture element of 3×3 configuring module, is detached. Wherever the full dark picture elements of the configuring module overlay with picture element on the feedback binary image validate dark the pixel of the subsequent object that relays to the configuring module. The resulting binary image is dilated, if OR calculation of these picture elements is certain, and the resulting binary image is eroded, if AND calculation of these picture elements is occupied.

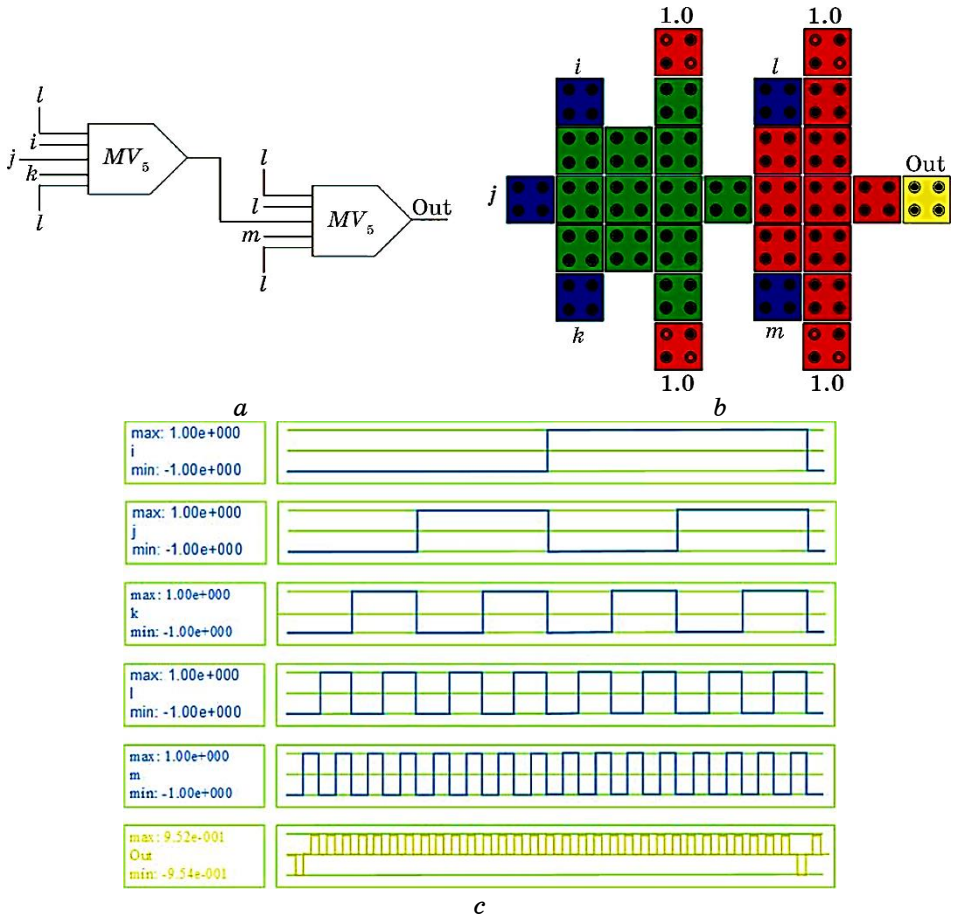

Fig. 4. QCA formation of designed non-configurable circuit: *a*—QCA schematic; *b*—QCA representation; *c*—outcome.

The designed architecture is drawn in Fig. 4, *a* and *b*, separately and the consistent outcome is given in Fig. 4, *c* where, it is coherent that the outlined process operates applicably. The outcome square is 1 (elevate), if each feedback is elevated excluding input *i*.

An innovative configurable design is also projected which contains 5 inputs as drawn in Fig. 5, *a* and *b*, separately. The computer simulation outcome is presented in Fig. 5, *c*, which authorizes the precision of the designed nanoarchitecture. As of the simulation process, it can be perceived that the outcome square is 0 (drop), if each feedback is elevated excluding input *i*.

A systematic calculation in state-of-the art and the designed architectures is provided in Table 1 and the productivity of the de-

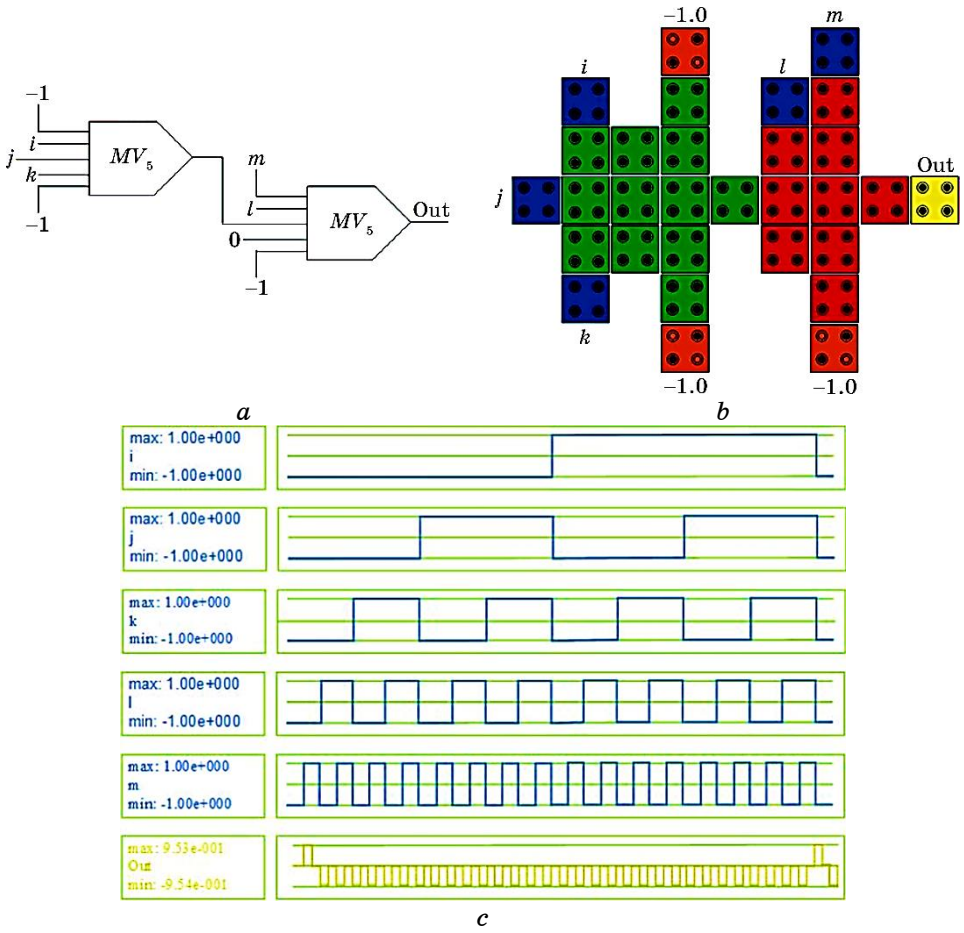

Fig. 5. QCA formation of designed configurable circuit: *a*—QCA schematic; *b*—QCA representation; *c*—outcome.

TABLE 1. Valuation of designed QCA nanoarchitectures.

Architecture	Employed cell	Extent in, μm^2	Clock cycle	Cell extent in, μm^2
Non-configure in [33]	35	0.044	3	0.01136
This paper	31	0.031	2	0.01007
Configure in [30]	51	0.051	4	0.01654
This paper	30	0.031	2	0.00976

signed architectures is certain from assessment. The outlined non-configurable nanoarchitecture achieved 12.42, 31.24, 34.36 and 12.45% improvement in terms of employed cell, enclosed extent, clock, and cell extent, respectively. Likewise, the configurable nanoarchitecture achieved 42.20, 41.18, 50.00 and 60.84% enhancement in terms of employed cell, enclosed extent, clock and cell extent, correspondingly.

5. ENERGY DISSIPATION OF THE DESIGNED NANOCIRCUITS

Designing QCA nanoarchetype circuits, the comprehensive energy of a cell is measured through Hamiltonian matrix [34, 35]. Used for a group of cells, the matrix and Hartree–Fock assessment with the columbic interaction regarding cells by a matrix explanation are stated in Refs. [36, 37]. Now from Eq. (4), M_i directs the overall emission f the i^{th} adjoining cell, $h_{i,j}$ is the numerical phase defining electrostatic control inside m and n cells reliable with the numerical plot, γ is the channelling energy concerning two logic phases of a QCA cell in addition Σ_i is the comprehensive amount adjoining the cells;

$$H = \begin{bmatrix} \dfrac{-E_k}{2}\sum_i M_i h_{m,n} & -\gamma \\ -\gamma & \dfrac{E_k}{2}\sum_i M_i h_{m,n} \end{bmatrix}. \tag{4}$$

The energy consumption can be nominal by calculating and completely;

$$P_{diss} = \frac{E_{diss}}{T_{cc}}\left\langle \frac{\hbar}{2T_{cc}}\Gamma_+\left[\frac{\Gamma_-}{|\Gamma_-|}\tanh\left(\frac{\hbar|\Gamma_-|}{K_cT}\right) - \frac{\Gamma_+}{|\Gamma_+|}\tanh\left(\frac{\hbar|\Gamma_+|}{K_cT}\right)\right]\right\rangle. \tag{5}$$

TABLE 2. Inclusive energy consumed through the designed nanocircuits at specific energy phase.

Outlined nanoarchitectures	Average energy consumed in, meV	Energy consumption at $T = 2$ K		
		$0.50E_k$	$1.0E_k$	$1.5E_k$
Non-configurable	Leakage energy	0.00828	0.02317	0.04096
	Switching energy	0.05448	0.05200	0.04524
	Energy consumption	0.06276	0.07517	0.08620
Configurable	Leakage energy	0.00836	0.02304	0.04027
	Switching energy	0.05148	0.04716	0.04261
	Energy consumption	0.05984	0.07020	0.08288

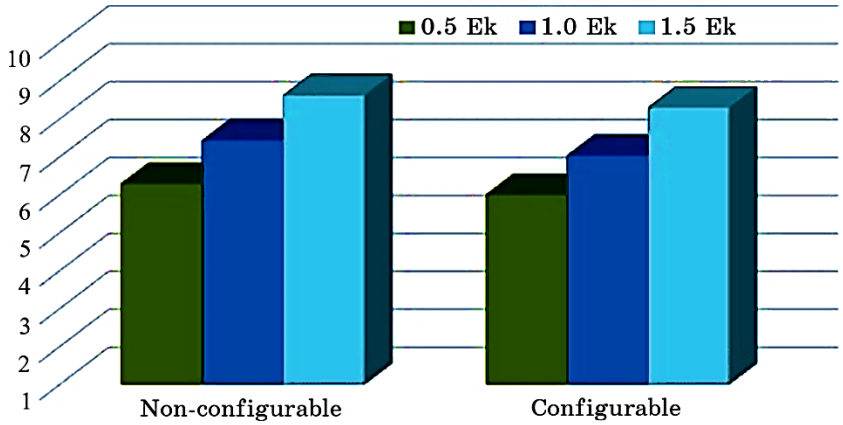

Fig. 6. Inclusive energy consumption at three different tunnelling phase where $T = 2$ K.

In Equation (5), Γ_+ and Γ_- defines the Hamiltonian values earlier and afterward the adjustment, T denotes the temperature, and K_c is the Boltzmann element. Overall energy consumption of the outlined nanoarchitectures is estimated through QCAPro simulation engine [35, 36]. The simulation engine evaluates the depleted energy of inclusive layout all design in a number of energy levels under non-adiabatic converting [37]. Total energy consumption is estimated at three specific channelling points is provided in Table 2 at a firm temperature of 2 K.

Figure 6 shows overall energy consumption for several tunnelling

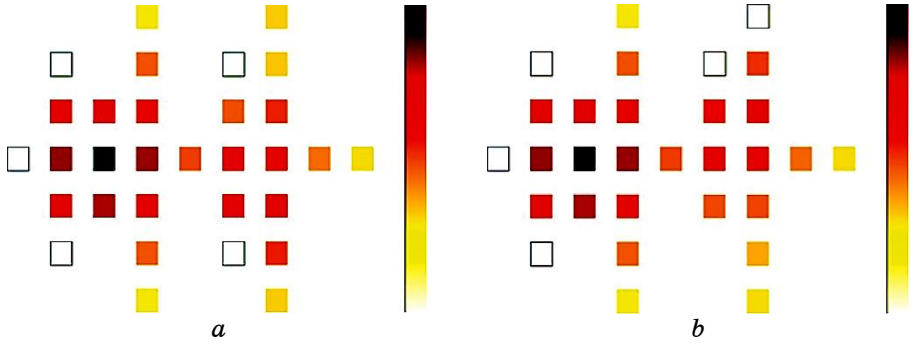

Fig. 7. The energy emission plots of designed (*a*) non-configurable and (*b*) configurable nanoarchitectures with $1.0E_k$ tunnelling energy at $T = 2$ K.

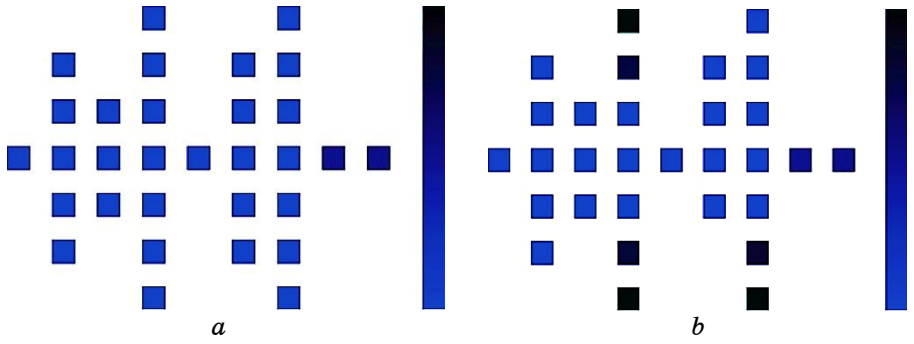

Fig. 8. The emission plots of designed (*a*) non-configurable and (*b*) configurable nanoarchitectures with $1.0E_k$ tunnelling energy at $T = 2$ K.

phase at a firm temperature of 2 K. The diagram shows that the inclusive energy consumption growths steadily for practical tunnelling level in the proposed nanoarchitectures.

The energy consumption map with $1.0E_k$ tunnelling energy at temperature of 2 K is provided in Fig. 7 mutually considering configurable and non-configurable nanocircuits.

Besides, Figure 8 presents the emission plots for both nanoarchitectures.

The temperature level effect on the output emission of proposed nanoarchitectures is achieved in this study. The output emission is occupied at several temperatures with QCADesigner engine. The average emission for every QCA cell is analysed from [14, 18] and systematized in Fig. 9. The structures perform proficiently in a temperature level of 1–11 K, and the emission for QCA cell is altered slightly in this level.

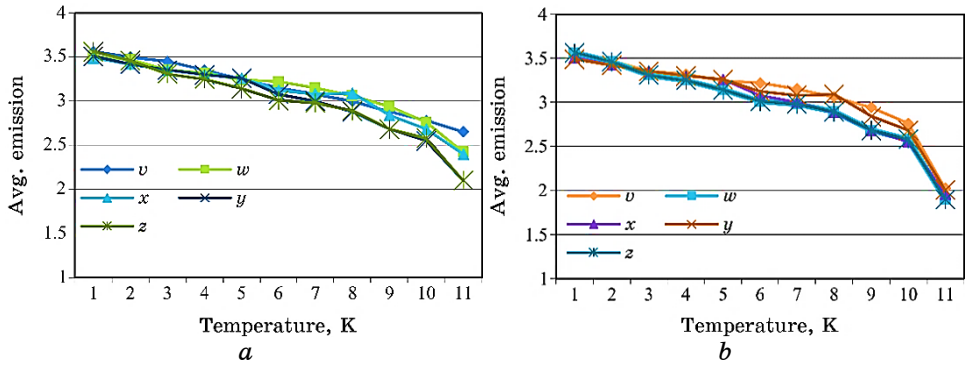

Fig. 9. Temperature *vs.* output emission; (*a*) non-configurable and (*b*) configurable nanoarchitectures.

6. CONCLUSION

In this research, the design and computer simulation of the MM configurable and non-configurable nanoarchitectures of dilation and erosion on digital binary images are analysed. The designed nanocircuits provide enhanced design achievement, comparable dispensation with minimal energy consumption related to state-of-the art nanoarchitectures. The simulation outcomes confirm the precise performance of the designed layouts. Moreover, the energy consumption by the architectures indicates that depleted energy level is rather minimal. This assists to form the proposed nanoarchitectures appropriating image processing operations practical on independent or cellular appliances.

REFERENCES

1. J. A. Carballo, W. T. J. Chan, P. A. Gargini, A. B. Kahng, and S. Nath, *32nd International Conference on Computer Design (ICCD) (19 October, 2014)*, p. 139; https://doi.org/10.1109/ICCD.2014.6974673
2. C. S. Lent, P. D. Tougaw, W. Porod, and G. H. Bernstein, *Nanotechnology*, **4**, Iss. 1: 49 (1993); https://doi.org/10.1088/0957-4484/4/1/004
3. N. Gallagher and G. Wise, *IEEE Trans. Acoust., Speech, Signal Process*, **29**, Iss. 6: 1136 (1981); https://doi.org/10.1109/TASSP.1981.1163708
4. E. Aptoula and S. Lefиvre, *Pattern Recognit*, **40**, Iss. 11: 2914 (2007); https://doi.org/10.1016/j.patcog.2007.02.004
5. I. Grattan-Guinness, *Hist. Math*, **31**, Iss. 2: 163 (2004); https://doi.org/10.1016/S0315-0860(03)00032-6
6. K. Michielsen and H. De Raedt, *Phys. Rep.*, **347**, Iss. 6: 461 (2001); https://doi.org/ 10.1016/S0370-1573(00)00106-X
7. V. Chatzis and I. Pitas, *IEEE Trans Image Process*, **19**, Iss. 7: 699 (2000);

https://doi.org/10.1109/42.875192
8. K. Benkrid, A. Benkrid, and S. Belkacemi, *J. Syst. Archit.*, **53**, Iss. 4: 184 (2007); https://doi.org/10.1016/j.sysarc.2006.09.010
9. K. Konstantinidis, G. C. Sirakoulis, and I. Andreadis, *IEEE Trans. Syst. Man Cybern, Pt. C*, **39**, Iss. 5: 520 (2009); https://doi.org/10.1109/TSMCC.2009.2020511
10. T. Cole and J. C. Lusth, *Prog. Quantum. Electron*, **25**, Iss. 4: 165 (2001); https://doi.org/10.1016/S0079-6727(01)00007-6
11. M. Abdullah-Al-Shafi and A. N. Bahar, *5th Intl. Conf. on Informatics, Electronics & Vision (May 13, 2016)*, p. 620; https://doi.org/10.1109/ICIEV.2016.7760076
12. P. D. Tougaw and C. S. Lent, *J. Appl. Phys.*, **75**, Iss. 3: 1818 (1994); https://doi.org/10.1063/1.356375
13. M. Abdullah-Al-Shafi and A. N. Bahar, *Cogent. Eng.*, **3**, Iss. 1: 1237864 (2016); https://doi.org/10.1080/23311916.2016.1237864
14. M. Abdullah-Al-Shafi, *Nanosistemi, Nanomateriali, Nanotehnologii*, **16**, Iss. 2: 289 (2018); http://dx.doi.org/10.15407/nnn.16.02.289
15 M. Abdullah-Al-Shafi, M. S. Islam, and A. N. Bahar, *Int. J. Comput. Appl.*, **128**, Iss. 2: 27 (2015); https://doi.org/10.5120/ijca2015906434
16. M. Abdullah-Al-Shafi, A. N. Bahar, F.Ahmad, and K. Ahmed, *Cogent. Eng.*, **4**, Iss. 1: 1349539 (2017); https://doi.org/10.1080/23311916.2017.1349539
17. M. Abdullah-Al-Shafi and A. N. Bahar, *Cogent. Eng.*, **4**, Iss. 1: 1391060 (2017); https://doi.org/10.1080/23311916.2017.1391060
18. M. Abdullah-Al-Shafi and A. N. Bahar, *J. Nanoelectron. Optoelectron.*, **13**, Iss. 6: 856 (2018); https://doi.org/10.1166/jno.2018.2302
19. M. Abdullah-Al-Shafi and A. N. Bahar, *Int. Nano Lett.*, **9**, Iss. 3: 265 (2019); https://doi.org/10.1007/s40089-019-0279-1
20. M. Abdullah-Al-Shafi and A. N. Bahar, *J. Comput. Theor. Nanosci.*, **14**, Iss. 5: 2416 (2017); https://doi.org/10.1166/jctn.2017.6842
21. M. Abdullah-Al-Shafi and A. N. Bahar, *Sens. Lett.*, **17**, Iss. 7: 595 (2019); https://doi.org/10.1166/sl.2019.4117
22. M. Abdullah-Al-Shafi and A. N. Bahar, *J. Nanoelectron. Optoelectron.*, **14**: Iss. 9: 1275 (2019); https://doi.org/10.1166/jno.2019.2630
23. M. Abdullah-Al-Shafi and Z. Rahman, *Solid State Electron. Lett.*, **1**, Iss. 2: 73 (2019); https://doi.org/10.1016/j.ssel.2019.11.004
24. M. Abdullah-Al-Shafi, A. N. Bahar, M. A. Habib, M. M. R. Bhuiyan, F. Ahmad, P. Z. Ahmad, and K. Ahmed, *Ain Shams Eng. J.*, **9**, Iss. 4: 2641 (2018); https://doi.org/10.1016/j.asej.2017.05.010
25. M. T. Niemier, M. J. Kontz, and P. M. Kogge, *Proc. 37th Annual Design Automation Conference (2000)*, p. 227; https://doi.org/10.1145/337292.337398
26. M. Crocker, X. S. Hu, M. Niemier, M. Yan, and G. Bernstein, *IEEE Trans. Nanotechnol.*, **7**, Iss. 3: 376 (2008); https://doi.org/10.1109/TNANO.2007.915022
27. M. Abdullah-Al-Shafi and A. N. Bahar, *Int. J. Inf. Technol. Comput. Sci.*, **10**, Iss. 10: 38 (2018); https://doi.org/10.5815/ijitcs.2018.10.05
28. Md. Abdullah-Al-Shafi, *Commun. Appl. Electron.*, **4**, Iss. 1: 20 (2016); http://dx.doi.org/ 10.5120/cae2016652004
29. J. L. Cardenas-Barrera, K. N. Plataniotis, and A. N. Venetsanopoulos,

Math. Probl. Eng., **8**, Iss. 1: 87 (2002); https://doi.org/10.1080/10241230211381
30. V. Mardiris and V. Chatzis, *J. Eng. Sci. Technol. Rev.*, **9**, Iss. 2: 25 (2016); https://doi.org/10.25103/jestr.092.05
33. R. Zhang, K. Walus, W. Wang, and G. A. Jullien, *IEEE Trans. Nanotechnol.*, **3**, Iss: 4: 443 (2004); https://doi.org/10.1109/TNANO.2004.834177
34. I. Amlani, A. O. Orlov, R. K. Kummamuru, G. H. Bernstein, C. S. Lent, and G. L. Snider, *Appl. Phys. Lett.*, **77**, Iss. 5: 738 (2000); https://doi.org/10.1063/1.127103
35. S. B. Tripathi, A. Narzary, R. Toppo, M. Goswami, and B. Sen, *J. Phys. Conf. Ser.*, **1039**, Iss. 1: 012028 (2018); https://doi.org/10.1088/1742-6596/1039/1/012028
36. M. Abdullah-Al-Shafi and R. Ziaur, *Solid State Electron. Lett.*, **1**, Iss. 2: 73 (2019); https://doi.org/10.1016/j.ssel.2019.11.004
37. S. Sheikhfaal, S. Angizi, S. Sarmadi, M. H. Moaiyeri, and S. Sayedsalehi, *Microelectron. J.*, **46**, Iss.6: 462 (2015); https://doi.org/10.1016/j.mejo.2015.03.016
38. S. S. Ahmadpour, M. Mosleh, and S. Rasouli Heikalabad, *J. Supercomput.*, **76**, Iss. 12: 10155 (2020); https://doi.org/10.1007/s11227-020-03249-3
39. M. Abdullah-Al-Shafi, M. S. Islam, and A. N. Bahar, *Int. Nano Lett.*, **10**, Iss. 3: 177 (2020); https://doi.org/10.1007/s40089-020-00304-y
40. M. R. Hasan, R. Guest, and F. Deravi, *ACM Comput. Surv.*, **55**, Iss. 13: 1 (2023); https://doi.org/10.1145/3583135